

Double Check My Desired Return: Transformer with Target Alignment for Offline Reinforcement Learning

Yue Pei¹, Hongming Zhang², Chao Gao², Martin Müller²,
Mengxiao Zhu¹, Hao Sheng¹, Haogang Zhu^{1*}, Liang Lin³

¹Beihang University, ²University of Alberta, ³Sun Yat-sen University

Abstract

Offline reinforcement learning (RL) has achieved significant advances in domains such as robotic control, autonomous driving, and medical decision-making. Most existing methods primarily focus on training policies that maximize cumulative returns from a given dataset. However, many real-world applications require precise control over policy performance levels, rather than simply pursuing the best possible return. Reinforcement learning via supervised learning (RvS) frames offline RL as a sequence modeling task, enabling the extraction of diverse policies by conditioning on different desired returns. Yet, existing RvS-based transformers, such as Decision Transformer (DT), struggle to reliably align the actual achieved returns with specified target returns, especially when interpolating within underrepresented returns or extrapolating beyond the dataset. To address this limitation, we propose *Doctor*, a novel approach that **Double Checks** the Transformer with target alignment for **Offline RL**. *Doctor* achieves superior target alignment both within and beyond the dataset, while enabling accurate and flexible control over policy performance. Notably, on the dynamic treatment regime benchmark, EpiCare, our approach effectively modulates treatment policy aggressiveness, balancing therapeutic returns against adverse event risk.

1 Introduction

In recent years, offline reinforcement learning (RL) has made remarkable progress in various domains, including robotic control (Fu et al. 2020; Levine et al. 2020), autonomous driving (Jiang et al. 2025), and medical decision-making (Hargrave, Spaeth, and Grosenick 2024). Most existing methods primarily aim to maximize the cumulative returns achieved by the learned agent, seeking to extract the best possible policy from a given offline dataset.

However, in many practical applications, it is necessary to precisely control the agent’s skill level in order to achieve different performance targets, rather than merely extracting the best-performing policy. For instance, AI clinicians need to carefully balance aggressive and conservative treatment strategies according to individual patient profiles (Rivenbark, O’Connor, and Coleman 2013), and educational AI assistants must dynamically adapt content and difficulty to match the abilities of different students (Singla et al. 2021).

*Corresponding author

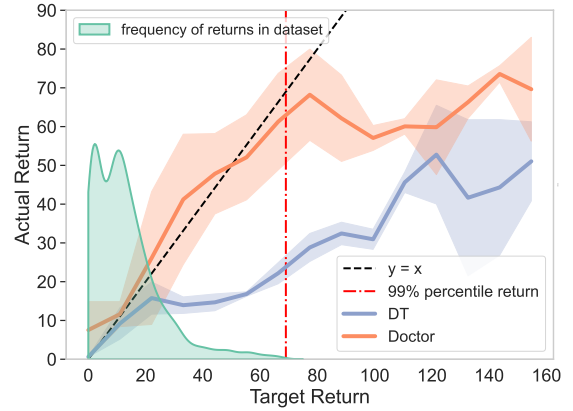


Figure 1: The actual returns achieved by *Doctor* and Decision Transformer (DT) conditioned on a wide range of target returns on the Hopper-Medium-Replay dataset. *Doctor* demonstrates significantly better alignment than DT, not only for well-supported returns within the dataset but also for extrapolated returns beyond the dataset.

Recent approaches have formulated offline RL as a sequence modeling problem analogous to large-scale language modeling, learning policies through self-supervised learning. This paradigm, known as reinforcement learning via supervised learning (RvS) (Emmons et al. 2021), predicts actions for each state in a supervised manner, conditioned on historical trajectories along with a target return prompt. By specifying the desired return as input, the learned transformer model is expected to output actions that achieve that particular return level (Chen et al. 2021; Janner, Li, and Levine 2021). Thus, RvS approaches enable the adjustment of policy by varying the target return prompt.

However, transformers trained via RvS typically struggle to align the achieved return with the specified target return. As illustrated in Figure 1, Decision Transformer (DT) (Chen et al. 2021), an RvS-based method, can successfully align returns only within the range of returns that are well-supported by the dataset. DT struggles to interpolate effectively across underrepresented return regions (left side of the dashed red line), and it also fails to reliably extrapolate to higher returns beyond those observed in the training data (right side of the dashed red line). This limitation suggests that training solely

with RvS is insufficient for learning policies whose actual returns closely match specified targets. Therefore, developing methods that explicitly perform target alignment is essential to accurately extract desired policies from an offline dataset, thus significantly benefiting a variety of offline RL applications. Nonetheless, existing work addressing precise target alignment in offline RL remains relatively limited.

To fill this research gap, we aim to address the target alignment problem for RvS transformers, namely, precisely controlling the model to perform at different levels of expertise. We propose a novel method, *Doctor*, which **Double Checks the Transformer** with target alignment for Offline RL. At inference time, we introduce a double-check mechanism that first generates a diverse set of candidate actions by scaling outputs conditioned on sampled returns and then estimates these actions using learned value functions, selecting the action whose associated value prediction most closely aligns with the specified target. This mechanism effectively broadens the return coverage and improves alignment for underrepresented or unseen target returns. In summary, our contributions are as follows.

(1) We introduce a novel double-check mechanism at inference time that significantly enhances target alignment. By generating multiple actions conditioned on sampled returns and validating these candidates using value functions, *Doctor* improves the model interpolation within underrepresented returns and extrapolation beyond the dataset.

(2) We demonstrate that the precise target alignment enables accurate control over the expertise of the policy, providing benefits for the medical RL. Specifically, on the dynamic treatment regime benchmark EpiCare (Hargrave, Spaeth, and Grosenick 2024), *Doctor* effectively modulates the aggressiveness of treatment policies, flexibly balancing therapeutic efficacy against adverse event risk.

(3) We empirically evaluate *Doctor* on offline RL benchmarks, including D4RL (Fu et al. 2020) and EpiCare. *Doctor* achieves superior target alignment both within and beyond the dataset. Furthermore, in terms of return maximization, *Doctor* achieves competitive results compared to existing methods, showing its effectiveness in a wide range of tasks.

2 Related Work

In this section, we review methods related to our approach and delineate the key distinctions between our method and these existing techniques.

Value Function Learning in Offline RL. Offline reinforcement learning only uses existing data collected by unknown policies without additional online data collection. One line of work is based on temporal difference (TD) learning (Zhang and Yu 2020; Fujimoto, Meger, and Precup 2019; Wu, Tucker, and Nachum 2019; Kumar et al. 2019, 2020; Sutton and Barto 2018; Dong, Ding, and Zhang 2020). To constrain the distance between the learned policy and the behavior policy to avoid distributional shift, they use a conservative value function to estimate the value of actions either by adding a regularization term in TD learning (Wu, Tucker, and Nachum 2019; Nair et al. 2020; Fujimoto and Gu 2021; Wu et al. 2022), or updating the value function in an in-sample manner (Zhou, Bajracharya, and Held 2021;

Kostrikov, Nair, and Levine 2022; Zhang et al. 2023; Xiao et al. 2023). These methods aim to extract the best possible policy from the existing dataset. Unlike these approaches, *Doctor*’s target alignment enables the model to perform at multiple skill levels, thereby benefiting offline RL.

Sequence Modeling based methods for Offline RL. Another line of work is Reinforcement Learning via Supervised Learning (RvS). These methods cast offline RL as a conditional sequence modeling problem and learn a policy auto-regressively. These approaches (Wang, Hunt, and Zhou 2022; Lee et al. 2022; Liu and Abbeel 2023; Wu, Wang, and Hamaya 2023; Hansen-Estruch et al. 2023; Chen et al. 2023; Chebotar et al. 2023; Ma et al. 2024; Kim et al. 2024) commonly condition on goals and expect that the derived policy could be improved by feeding a high goal, but struggle to align the actual return with the desired target.

RADT (Tanaka et al. 2024) aims to address return alignment by introducing specialized aligners, which overcomes the limitations of attention allocation. RADT focuses on improving the network architecture, whereas *Doctor* introduces enhancements in the learning and inference methodology; thus, the two methods are orthogonal. Moreover, RADT evaluates return alignment by testing the absolute error, while *Doctor* empirically demonstrates that target alignment can directly benefit dynamic treatment regimes.

Recent RvS-based approaches, such as QDT (Yamagata, Khalil, and Santos-Rodriguez 2023), QT (Hu et al. 2024), CGDT (Wang et al. 2024), and ACT (Gao et al. 2024)—also leverage Q-values to augment transformer policies. However, these methods focus mainly on improving the model’s stitching ability to obtain the best policy from the dataset. In contrast, our primary objective is explicit target alignment, enabling an offline-trained transformer to accurately perform at different skill levels. Moreover, unlike prior work that depends on training-time Q-value regularization or critic-based prompts, the novelty of *Doctor* lies in the inference-time dynamic checking mechanism.

3 Preliminaries

Offline Reinforcement Learning

Reinforcement learning (RL) (Sutton and Barto 2018) is a paradigm of agent learning via interaction. It can be modeled as a Markov Decision Process (MDP), a 5-tuple $\mathcal{M} = (\mathcal{S}, \mathcal{A}, \mathcal{R}, P, \gamma)$. \mathcal{S} denotes the state space, \mathcal{A} denotes the action space, $P(s'|s, a) : \mathcal{S} \times \mathcal{A} \times \mathcal{S} \rightarrow [0, 1]$ is the environment dynamics, $\mathcal{R}(s, a) : \mathcal{S} \times \mathcal{A} \rightarrow \mathbb{R}$ is the reward function which is bounded, $\gamma \in [0, 1]$ is the discount factor. Consider the finite horizon setting, the agent interacts with the environment for T steps. Denote the state, action and reward at timestep t as s_t, a_t and r_t , a trajectory is a sequence of states, actions and rewards $\tau := (s_0, a_0, r_0, s_1, a_1, r_1, \dots, s_T, a_T, r_T)$. The return at timestep t is defined as $R_t = \sum_{i=t}^T \gamma^{i-t} r_i$. The goal of an reinforcement learning agent is to learn an optimal policy π that maximizes the expected return $R_0 = \mathbb{E}_\pi[\sum_{i=0}^T \gamma^i r_i]$.

In offline RL, instead of interacting with the environment, the agent learns from a static dataset of trajectories $\mathcal{D} := \{\tau_j\}$ such as the D4RL benchmark (Fu et al. 2020).

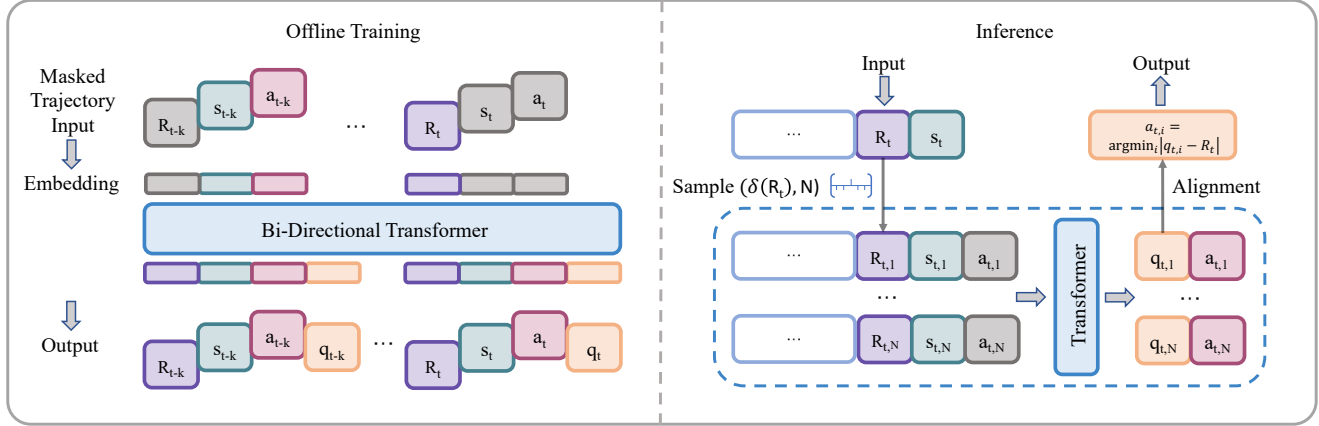


Figure 2: An overview of *Doctor*. **Left.** The training involves reconstructing the original trajectory and estimating the action-value from a partial, randomly masked trajectory. Returns, states and actions are fed into modality-specific embeddings and then processed by the transformers. The value heads estimate the action-value at each timestep. **Right.** At inference time, *Doctor* samples actions around the target return and validates them with the value head outputs to ensure alignment.

Several recent offline-RL methods impose an in-sample constraint (Levine et al. 2020), learning Q-functions over the dataset’s state–action visitation:

$$Q(s, a) \leftarrow r + \gamma \max_{(s', a') \in \mathcal{D}} Q(s', a'). \quad (1)$$

For example, Implicit Q-Learning (IQL) (Kostrikov, Nair, and Levine 2022) only bootstraps from actions seen in the dataset, avoiding value estimates on unseen actions and substantially reducing estimation error. This setting eliminates the need for online exploration, which is practical in scenarios where exploration is expensive or dangerous.

Reinforcement Learning via Supervised Learning.

Decision Transformer (DT) applies transformers to offline RL. Different from offline RL methods based on temporal difference learning, DT models offline RL as a sequence modeling problem and learns a policy auto-regressively by predicting the next action given the history trajectory conditioned on a target return. This set of approaches abstract offline RL as a sequence modeling problem and learns a policy via supervised learning (RvS). These approaches (Chen et al. 2021; Janner, Li, and Levine 2021) frame offline RL as a sequence modeling problem. The K-step historical trajectory sequence τ_t consists of three modalities:

$$\tau_t = (R_{t-K+1}, s_{t-K+1}, a_{t-K+1}, \dots, R_t, s_t, a_t), \quad (2)$$

where R_t is the (discounted) return at time step t , s_t is the state, and a_t is the action. These methods condition on goals or target returns and expect that the derived policy could be improved when feeding a high-goal or large-return.

4 Method

In this section, we introduce our method, *Doctor*. We first introduce our model architecture and describe how the model is trained to predict value and actions. We then introduce a double-check mechanism at inference time to improve alignment. Figure 2 illustrates the overall framework.

Model Architecture

Our model adopts an encoder-decoder architecture as a universal representation extractor. Both the encoder and decoder are bidirectional transformers, which are adept at capturing dependencies in sequential data. The task is based on sequence reconstruction from masked views (He et al. 2022; Vaswani 2017; Kitaev, Kaiser, and Levskaya 2020), where a random subset of the sequence is masked and the model is tasked with reconstructing the original trajectory.

This design choice is motivated by recent work (Wu et al. 2023) which demonstrated that bidirectional transformers trained with random and auto-regressive masking encourage the model to reconstruct missing tokens by leveraging the context of the unmasked sequence, enhancing the generalization. We expect this design to yield stronger interpolation when handling trajectories associated with underrepresented returns. Our experiments (Figure 4 and Appendix E.2) confirm that the bidirectional transformer-based architecture achieves improved target alignment.

As illustrated in the left of Figure 2, we apply random and auto-regressive mask M to certain elements of the sequence,

$$M(\tau_t) = (R_{t-K+1}, _, a_{t-K+1}, _, s_{t-K+2}, _, \dots _, s_T, _), \quad (3)$$

where the masked elements are denoted as $_$. The masked sequence $M(\tau_t)$ is then fed into the encoder-decoder architecture E and D to obtain the last layer’s latent representation $\tau^z = D(E(M(\tau_t)))$. A linear layer for each modality is applied to the latent representation τ^z to predict the return, state, and action at each timestep.

Along with reconstructing the trajectory, the latent representation τ^z is also used to predict the action-value q_t at each timestep. τ^z integrates the information from multiple timesteps, which is beneficial for partial observability in RL tasks. And the action-value q_t endows the model with the ability to evaluate the return. At inference time, we fed the unmasked full trajectory into the model to obtain the predicted actions and action-values.

Training

Our training consists of two purposes: (1) reconstructing the original trajectory sequence from the masked input trajectory, and (2) learning the action-value q_t to double check the candidates to improve alignment.

Denoting the learnable parameters of embeddings and the encoder-decoder as θ , inducing conditional probabilities as P_θ , the objective is to minimize the negative log-likelihood of the original trajectory sequence given the masked input:

$$\mathcal{L}_{\text{recon}}(\theta) = - \sum_{t=0}^T \left(\log P_\theta(R_t | M(\tau_t)) + \log P_\theta(s_t | M(\tau_t)) + \log P_\theta(a_t | M(\tau_t)) \right). \quad (4)$$

Besides reconstructing the trajectory, the model is also trained to predict the action-value q_t . Our Q function includes individual Q head at each timestep, corresponding to the state action pairs. It takes the latent trajectory representation τ^z as input and outputs action-value estimates. This enables the Q function to leverage the rich representations learned from the reconstruction task.

The goal of the Q function is to learn an optimal action-value function, aligning with target returns. To avoid querying the learned Q function on out-of-sample actions, we utilize the asymmetric least squares loss function (Kostrikov, Nair, and Levine 2022). Denote the learnable parameters of the Q function as ϕ . The learning loss is defined by:

$$\mathcal{L}_Q(\phi) = \sum_{t=0}^{T-1} L_2^\nu(r_t + \gamma Q_{\phi, t+1}(\tau^z, a_{t+1}) - Q_{\phi, t}(\tau^z, a_t)), \quad (5)$$

where r_t is the reward, γ is the discount factor, $Q_{\phi, t}$ and $Q_{\phi, t+1}$ are the Q functions at time step t and $t+1$, respectively. $L_2^\nu(u) = |\nu - 1(u < 0)|u^2$ is the asymmetric least squares loss function. For $\nu = 0.5$, the loss function is equivalent to the standard mean squared error loss. For $\nu > 0.5$, the loss function is asymmetric, which down-weights the contributions of values smaller than zero (Newey and Powell 1987; Kostrikov, Nair, and Levine 2022). Eq. (1) can be approximated with $\tau \approx 1$.

We initialize Q functions Q_ϕ and train them jointly with the transformers. The overall objective is to minimize the sum of the reconstruction loss and the TD loss:

$$\mathcal{L}(\theta, \phi) = \mathcal{L}_{\text{recon}}(\theta) + \mathcal{L}_Q(\phi). \quad (6)$$

Inference Time Alignment

Given a tuple (R_t, s_t, a_t, q_t) , the return R_t represents the return in the dataset when taking action a_t at state s_t , while the action-value q_t reflects the expected return. We expect there could be a gap between q_t and R_t . This gap presents the difference between policy evaluation of the unknown behavior policy that collected the dataset and the best possible policy after policy improvement. This motivates us to introduce a double-check mechanism during inference to ensure alignment between the predicted action and the target return.

Formally, given the current state s_t , denote R_t as the desired target return at timestep t . We define $\delta(R_t) := \{R : |R - R_t| \leq \delta\}$ as the set of returns within a distance δ from R_t . We sample N returns from $\delta(R_t)$ uniformly,

$$\{R_{t,1}, R_{t,2}, \dots, R_{t,N}\} \sim \text{Unif}(\delta(R_t), N), \quad (7)$$

and construct N trajectories by assigning $R_{t,i}$ to replace R_t in the original trajectory. We then feed these N trajectories into the transformer model:

$$\underbrace{\left\{ \begin{array}{l} (R_{t-K+1,i}, s_{t-K+1,i}, a_{t-K+1,i}) \\ \dots \\ (R_{t,i}, s_{t,i}, _) \end{array} \right\}_{i=1}^N}_{\text{input trajectories}} \rightarrow \underbrace{\left\{ \begin{array}{l} (R_{t-K+1,i}, s_{t-K+1,i}, a_{t-K+1,i}, q_{t-K+1,i}) \\ \dots \\ (R_{t,i}, s_{t,i}, a_{t,i}, q_{t,i}) \end{array} \right\}_{i=1}^N}_{\text{output trajectories}}, \quad (8)$$

where we obtain N predicted actions $\{a_{t,1}, a_{t,2}, \dots, a_{t,N}\}$ and their corresponding action-values $\{q_{t,1}, q_{t,2}, \dots, q_{t,N}\}$. To ensure alignment, we select the action with the nearest action-value to R_t as the final action:

$$a_{t,i} = \arg \min_{a_{t,i}} (|q_{t,i} - R_t|). \quad (9)$$

After taking action $a_{t,i}$ and obtaining the reward r_t , we updates the desired target return R_{t+1} to $(R_t - r_t)/\gamma$ and repeat the process for the next timestep. This double-check mechanism first ensures that the actions are sampled near the desired target return and then validates them using the action-values to ensure alignment. This mechanism enables the model to interpolate and extrapolate between underrepresented or missing returns in the dataset.

To achieve high returns, we can set an aggressive target return that even exceeds the best possible return. The model will sample actions based on this desired target and validate them with action-values, selecting the action with the highest value. Conversely, to obtain a specific moderate return, we can set that return as the target. The model will then double-check the predicted action, selecting the one with the value closest to the target return. We offer further justification of the double-check mechanism in Appendix C.1. We include the algorithm of *Doctor* in Appendix B.

5 Experiments

In the experiment section, we evaluate *Doctor* across multiple benchmarks to address three questions:

- Can *Doctor* generate actions that achieve closer alignment between actual returns and specified target returns compared to existing baseline methods?
- Can *Doctor* effectively support the policy control requirements in reinforcement learning applications, such as precisely adjusting the skill of the model to flexibly meet the varying treatment objectives in clinical decision-making scenarios?
- What is the impact of *Doctor*'s double-check mechanism on target alignment, and how does it translate into improvements in the final cumulative return?

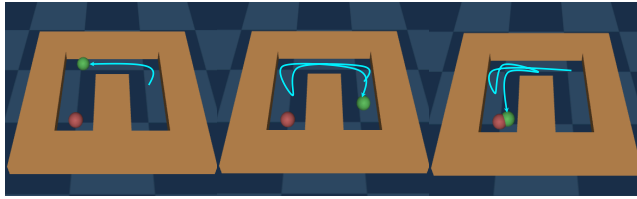


Figure 3: Trajectories generated under three different target returns, which are 10, 40 and 80, resulting in actual returns of 37.80, 46.85, and 80.16, respectively, from the left to right. As the target return increases, we observe that the agent is guided closer to the goal.

Setup

We use D4RL (Fu et al. 2020) and EpiCare (Hargrave, Spaeth, and Grosenick 2024) as our testbeds. More environmental details can be found in Appendix D.

- **D4RL.** D4RL consists of various robotic environments and datasets. We consider Locomotion-v2 tasks, as well as Maze2D-v1 and Adroit-v1 tasks. To address the questions comprehensively, we test our method against 11 representative baselines, that are state of the art in each categories. For value-based methods, we select CQL (Kumar et al. 2020), which adopts pessimistic action estimation. IQL (Kostrikov, Nair, and Levine 2022), an in-sample multi-step dynamic programming approach and policy regularization-based approach, TD3+BC (Fujimoto and Gu 2021). For RvS-based methods, we consider DT (Chen et al. 2021), MTM (Wu et al. 2023), RvS-R (Emmons et al. 2021) and RADT (Tanaka et al. 2024). And we evaluate advanced methods proposed to integrate RvS and TD learning. We include CGDT (Wang et al. 2024) and ACT (Gao et al. 2024), both aiming to improve RvS-trained Transformer-based policies through value functions. QT (Hu et al. 2024) enhances the stitching ability of DT by introducing the Q-value regularizer, achieving strong performance.
- **EpiCare.** EpiCare is an offline RL benchmark designed for dynamic treatment regimes (DTRs), simulating core challenges in longitudinal clinical settings. It incorporates short treatment horizons, heterogeneous treatment effects, partial observability, and adverse events. The offline dataset used for training is generated through simulated clinical trials, reflecting realistic data collection processes. In addition to cumulative returns, the benchmark also measures adverse event rates. For comparison, we adopt the methods provided by the EpiCare benchmark, BC (Torabi, Warnell, and Stone 2018), IQL (Kostrikov, Nair, and Levine 2022), TD3+BC (Fujimoto and Gu 2021), CQL (Kumar et al. 2020), and additionally implemented DT (Chen et al. 2021) and MTM (Wu et al. 2023) as our comparison baselines.

The Superiority of *Doctor* in Return Alignment

The key advantage of *Doctor* is its ability to achieve a wide range of desired target returns, an expected capability for return-conditioned models that most existing methods fail

to achieve. We first present a visual demonstration to illustrate the efficacy of target alignment achieved by *Doctor*. Specifically, we show the trajectory image recorded on the maze2d-umaze-dense task in Figure 3, providing a more intuitive representation compared to curve-based evaluations.

In this environment, the reward is the exponential negative Euclidean distance between the achieved goal position and the desired goal position:

$$r_t = \exp(-\|g_{\text{achieved},t} - g_{\text{desired}}\|_2), \quad (10)$$

where g_{desired} is the goal position, $g_{\text{achieved},t}$ is the achieved goal position at time step t . The horizon of an episode is 300. We evaluate *Doctor* under three different target returns, specifically 10, 40, and 80, depicted from left to right. The agent is guided to achieve an actual return that aligns with the target return, resulting in actual returns of 37.80, 46.85, and 80.16, respectively. We provide the complete trajectory plots of the agents in Appendix E.1.

Next, we evaluate the alignment ability of *Doctor* on the hopper-medium-replay-v2 dataset. We vary the level of suboptimality by removing top return trajectories from the dataset and test the model across a wide range of target returns. As suboptimality increases, the maximum returns of the trajectories in the dataset progressively decrease, moving the dataset further away from the optimal. We perform 140,000 gradient updates during training, and evaluate the model by rolling out 10 episodes. we set $N = 300$ and δ is small value fluctuating based on the maximum return in the dataset. Specifically, we choose $\delta = 5\% \times R_{\max}$. We report the final results over five random seeds.

We compare *Doctor* with DT, MTM and QT, Figure 4 shows the results. The x-axis represents the target return, the y-axis represents the actual return achieved in the environment. The dashed red line marks the max return in the dataset. The dashed black lines denote the ideal line that perfectly aligns with the target return. *Doctor* achieves significantly better alignment, more closely adhering to the ideal diagonal line, even when the target return exceeds the maximum return in the dataset to some extent. This indicates that *Doctor* can not only interpolate more effectively within the dataset but also facilitates extrapolation, allowing the model to achieve target returns accurately, even beyond those observed in the training data. Notably, bidirectional transformer based methods like MTM and *Doctor* lie closer to the diagonal than DT and QT, highlighting the architectural advantage in terms of target alignment. We provide more results in Appendix E.2 and test the error between the actual return and the target return in Appendix E.6.

The Advantage of *Doctor* in Clinical Policy Control

In this section, we demonstrate how *Doctor*'s superior alignment can benefit medical RL applications. To this end, we evaluate *Doctor* using the EpiCare benchmark. EpiCare benchmark provides datasets generated by distinct behavior policies across eight different environments (defined by environment seeds 1–8, each simulating diseases with different characteristics). We use the dataset generated by the Standard of Care (SoC) policy, which simulates clinician behavior by avoiding high-risk treatments based on symptom

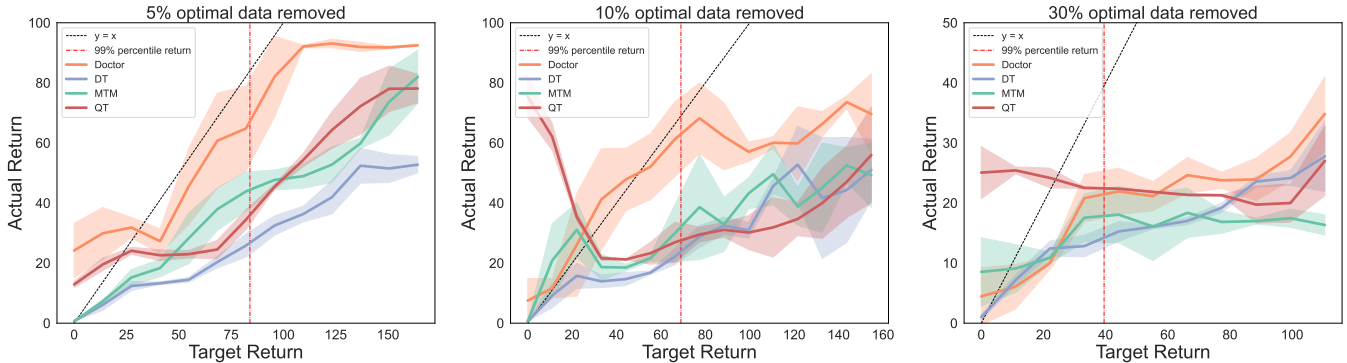


Figure 4: We evaluate the alignment ability of *Doctor* on the hopper-medium-replay-v2 with the top X% returns of trajectories removed. The dashed red line presents the highest return in the dataset. The dashed black lines denote the ideal alignment. *Doctor* achieves much better alignment across a wide range of target returns compared to DT, MTM and QT.

thresholds. Baseline methods are adapted to discrete control by optimizing logits of one-hot encoded action outputs. We evaluated the models online on 1,000 trajectories, measuring key metrics: clinical returns and adverse events.

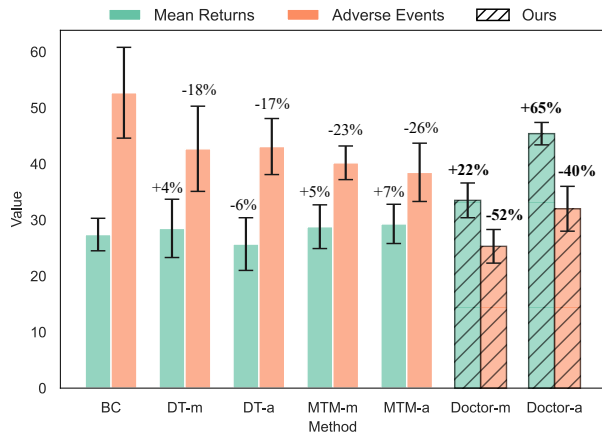


Figure 5: Mean returns and adverse-event rates per 10k episodes under moderate (m, 0.4x) and aggressive (a, 0.8x) targets (+/-% denote change vs. BC). Results are averaged over 3 seeds. Results show that (1) DT and MTM exhibit only marginal shifts relative to BC, while *Doctor* demonstrates significant improvements. (2) DT and MTM have minimal responsiveness to target changes. By contrast, *Doctor* can sensitively adjust its policy to meet specified targets.

Figure 5 reports clinical return and adverse events per 10k episodes under 0.4 and 0.8 times maximum returns in the datasets. The results demonstrate that (1) DT and MTM exhibit only marginal shifts relative to BC, while *Doctor* shows more significant improvements (improves returns by 22% / 65% and reduces adverse events by 52% / 40% at moderate / aggressive targets compared with BC). (2) DT and MTM have minimal response to target changes. By contrast, *Doctor* can control its policy with treatment aggressiveness, it achieves higher returns at the expense of higher adverse events under aggressive setting, while lower returns but mitigate adverse events under moderate targets.

igate adverse events under moderate targets.

This result demonstrates that *Doctor* can flexibly control the treatment policy between aggressive and conservative as a single unified model. Such controllability holds promise for clinical practice, allowing physicians to tailor interventions to each patient’s unique condition, choosing more aggressive therapies when potential benefit outweighs risk, or adopting conservative approaches to safeguard vulnerable individuals (Rivenbark, O’Connor, and Coleman 2013). We report a comparison of *Doctor* against baselines on the EpiCare benchmark in terms of mean returns and adverse event rate in Appendix E.5. *Doctor* achieves both higher returns and lower adverse event rate, indicating its advantages in treatment efficacy and safety.

The Impact of *Doctor*’s Double-Check Mechanism

We further analyze the impact of the sampling size N on the alignment ability of *Doctor* in this section. To investigate this, we conduct an ablation study on hopper-medium-replay-v2 task with 10% of the best data removed, testing N with increasing values in $\{2, 5, 10, 100, 300\}$.

As shown in Figure 6, when $N = 2$, the model utilizes an inference strategy akin to the RvS-based method, resulting in inferior alignment. This indicates that the target return alone is not sufficient to ensure alignment. As N increases, the model achieves better alignment, highlighting the importance of multiple samples for target return alignment and the effectiveness of the double-check mechanism. Sampling multiple returns around the target encourages the transformer to propose a rich variety of actions that map the local return, reducing conditioning noise. A subsequent value-function check then filters these candidates, selecting the action whose predicted return most closely matches the target, combining broad exploration with precise validation to achieve substantially tighter alignment.

Next, we perform an ablation study to quantify the contributions of *Doctor*’s components, random masking and the double-check mechanism on the MuJoCo medium datasets. Table 2 reports the mean absolute error averaged at multiple target returns between the actual return and the target return. When we remove the random-masking pattern (w/o RM),

Tasks	BC	CQL	IQL	TD3+BC	DT	MTM	RADT	RvS	CGDT	ACT	QT	<i>Doctor</i>
halfCheetah-MR	36.6	45.5	44.2	44.6	36.3	43.0	41.3	38.0	40.4	43.0	47.2	46.6 \pm 0.9
hopper-MR	18.1	95.0	94.7	60.9	82.7	92.9	95.7	73.5	93.4	98.4	96.1	98.8 \pm 2.1
walker2d-MR	26.0	77.2	73.9	81.8	66.6	77.3	75.9	60.6	78.1	56.1	91.5	86.2 \pm 2.6
halfCheetah-M	42.6	44.0	47.4	48.4	42.0	43.6	42.8	41.6	43.0	49.1	47.5	48.4 \pm 0.7
hopper-M	52.9	58.5	66.3	59.3	67.6	64.1	93.7	60.2	96.9	67.8	85.8	85.6 \pm 7.4
walker2d-M	75.3	72.5	78.3	83.7	74.0	70.4	75.6	71.7	79.1	80.9	84.6	81.1 \pm 2.7
halfCheetah-ME	55.2	91.6	86.7	90.7	86.8	94.7	93.1	92.2	93.6	96.1	93.3	95.8 \pm 0.5
hopper-ME	52.5	105.4	91.5	98.0	107.6	112.4	110.4	101.7	107.6	111.5	111.5	113.5 \pm 0.6
walker2d-ME	107.5	108.8	109.6	110.1	108.1	110.2	109.7	106.0	109.3	113.3	109.9	113.7 \pm 1.3
Locomotion Sum	466.7	698.5	692.6	677.5	671.7	708.6	738.2	645.5	741.4	716.2	767.4	769.7

Table 1: Offline results on the D4RL benchmark. *Doctor* achieves competitive results compared to the baselines, including RvS-based methods and TD learning-based methods, as well as advanced methods proposed to integrate RvS and TD learning. The best baselines are highlighted in bold for final performance.

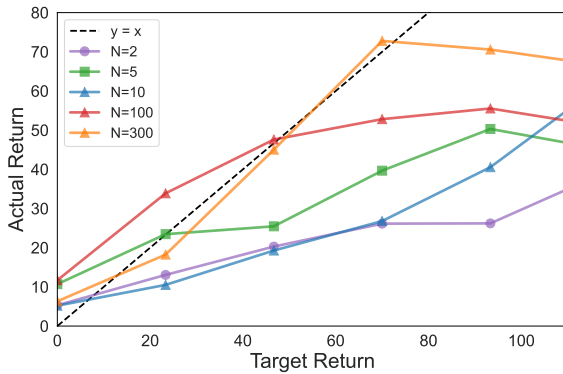


Figure 6: The effect of the sampling size N . As N increases, *Doctor* achieves better alignment with the target return.

Approach	halfcheetah-M	hopper-M	walker2d-M
w/o RM	32.3 ± 4.6	14.5 ± 2.4	24.1 ± 6.6
w/o DB	26.2 ± 5.1	12.9 ± 2.7	28.6 ± 7.3
Doctor	16.2 ± 5.8	10.4 ± 3.3	12.0 ± 8.1

Table 2: Absolute error comparison in the ablation study. Results are averaged over three seeds. Lower number is better.

errors rise, indicating that masking is critical to covering a broad return spectrum. Ablating the double-check mechanism (w/o DB) likewise degrades performance, showing its importance for alignment. The full model combining both yields the lowest error across all three tasks.

Inducing sampling may introduce extra computational overhead. We evaluate the inference and training time of different algorithms. For training, we use a batch size of 2048 for all four algorithms. We set sizes of hidden units as 256 for all the networks, measuring the time required to train one batch. For inference, we calculate the Frames Per Second (FPS) by running one episode, measuring the total time taken, and then dividing by the episode length. The reported values are the averages of 5 test runs, as shown in Table 3. It can be observed that *Doctor*'s computation overhead does not significantly increase. During inference, *Doc-*

Time Complexity	DT	MTM	QT	<i>Doctor</i>
Inference (seconds)	0.01	0.012	0.016	0.013
Training (seconds)	2.13	1.29	2.51	1.35

Table 3: Time Complexity for Algorithms

tor processes one batch at a time and leverages a unified architecture to generate both action predictions and value estimates simultaneously, allowing for fully parallel computation. *Doctor* uses a Q function trained with the transformer-based representation, and compared to the computational cost of the transformer itself, the additional cost of Q function computation is relatively low.

The Capability of *Doctor* in Return Maximization

We further assess the return maximization performance of *Doctor* in offline settings, presenting results averaged over five random seeds. As shown in Table 1, *Doctor* achieves competitive performance compared to the strongest baseline, QT, and outperforms other baselines by a substantial margin. QT demonstrates robust performance in maximizing the return, but it degrades interpolation accuracy and fails to maintain accurate alignment, as depicted in Figure 4, whereas *Doctor* consistently achieves superior alignment.

We report results on the Maze2d tasks that contain very few near-optimal trajectories in Appendix E.4, *Doctor* outperforms other baselines, showing its stitching ability. Furthermore, in a complex high-dimensional control task, Adroit, *Doctor* also achieves clear improvements, as shown in Appendix E.3. These results highlight *Doctor*'s effectiveness in a wide range of tasks.

6 Conclusion

In this work, we propose a novel method that double checks the transformer with target alignment for offline RL (*Doctor*). At inference time, we introduce a double-check mechanism to sample actions based on desired target returns and validate them with action-values to enhance alignment. Experiments demonstrate that *Doctor* achieves superior target alignment both within and beyond the dataset. This alignment can control treatment policies that balance the adverse event rate with therapeutic returns on EpiCare benchmark.

References

Brockman, G. 2016. OpenAI Gym. *arXiv preprint arXiv:1606.01540*.

Chebotar, Y.; Vuong, Q.; Hausman, K.; Xia, F.; Lu, Y.; Irpan, A.; Kumar, A.; Yu, T.; Herzog, A.; Pertsch, K.; et al. 2023. Q-transformer: Scalable offline reinforcement learning via autoregressive q-functions. In *Conference on Robot Learning*, 3909–3928. PMLR.

Chen, H.; Lu, C.; Wang, Z.; Su, H.; and Zhu, J. 2023. Score regularized policy optimization through diffusion behavior. *arXiv preprint arXiv:2310.07297*.

Chen, L.; Lu, K.; Rajeswaran, A.; Lee, K.; Grover, A.; Laskin, M.; Abbeel, P.; Srinivas, A.; and Mordatch, I. 2021. Decision transformer: Reinforcement learning via sequence modeling. *Advances in neural information processing systems*, 34: 15084–15097.

Dong, H.; Ding, Z.; and Zhang, S. 2020. *Deep Reinforcement Learning: Fundamentals, Research and Applications*. Springer Nature.

Emmons, S.; Eysenbach, B.; Kostrikov, I.; and Levine, S. 2021. Rvs: What is essential for offline rl via supervised learning? *arXiv preprint arXiv:2112.10751*.

Fu, J.; Kumar, A.; Nachum, O.; Tucker, G.; and Levine, S. 2020. D4rl: Datasets for deep data-driven reinforcement learning. *arXiv preprint arXiv:2004.07219*.

Fujimoto, S.; and Gu, S. S. 2021. A minimalist approach to offline reinforcement learning. *Advances in neural information processing systems*, 34: 20132–20145.

Fujimoto, S.; Meger, D.; and Precup, D. 2019. Off-policy deep reinforcement learning without exploration. In *International Conference on Machine Learning*, 2052–2062. PMLR.

Gao, C.-X.; Wu, C.; Cao, M.; Kong, R.; Zhang, Z.; and Yu, Y. 2024. ACT: empowering decision transformer with dynamic programming via advantage conditioning. In *Proceedings of the AAAI Conference on Artificial Intelligence*, volume 38, 12127–12135.

Hansen-Estruch, P.; Kostrikov, I.; Janner, M.; Kuba, J. G.; and Levine, S. 2023. Idql: Implicit q-learning as an actor-critic method with diffusion policies. *arXiv preprint arXiv:2304.10573*.

Hargrave, M.; Spaeth, A.; and Grosenick, L. 2024. EpiCare: A Reinforcement Learning Benchmark for Dynamic Treatment Regimes. *Advances in Neural Information Processing Systems*, 37: 130536–130568.

He, K.; Chen, X.; Xie, S.; Li, Y.; Dollár, P.; and Girshick, R. 2022. Masked autoencoders are scalable vision learners. In *Proceedings of the IEEE/CVF conference on computer vision and pattern recognition*, 16000–16009.

Hu, S.; Fan, Z.; Huang, C.; Shen, L.; Zhang, Y.; Wang, Y.; and Tao, D. 2024. Q-value regularized transformer for offline reinforcement learning. *arXiv preprint arXiv:2405.17098*.

Janner, M.; Li, Q.; and Levine, S. 2021. Offline reinforcement learning as one big sequence modeling problem. *Advances in neural information processing systems*, 34: 1273–1286.

Jiang, B.; Chen, S.; Zhang, Q.; Liu, W.; and Wang, X. 2025. Alphadrive: Unleashing the power of vlm in autonomous driving via reinforcement learning and reasoning. *arXiv preprint arXiv:2503.07608*.

Kaelbling, L. P.; Littman, M. L.; and Cassandra, A. R. 1998. Planning and acting in partially observable stochastic domains. *Artificial intelligence*, 101(1-2): 99–134.

Kim, J.; Lee, S.; Kim, W.; and Sung, Y. 2024. Adaptive q-aid for conditional supervised learning in offline reinforcement learning. *Advances in Neural Information Processing Systems*, 37: 87104–87135.

Kitaev, N.; Kaiser, L.; and Levskaya, A. 2020. Reformer: The Efficient Transformer. In *International Conference on Learning Representations*.

Kostrikov, I.; Nair, A.; and Levine, S. 2022. Offline Reinforcement Learning with Implicit Q-Learning. In *International Conference on Learning Representations*.

Kumar, A.; Fu, J.; Soh, M.; Tucker, G.; and Levine, S. 2019. Stabilizing off-policy q-learning via bootstrapping error reduction. *Advances in Neural Information Processing Systems*, 32.

Kumar, A.; Zhou, A.; Tucker, G.; and Levine, S. 2020. Conservative Q-learning for offline reinforcement learning. *Advances in Neural Information Processing Systems*, 33: 1179–1191.

Lee, K.-H.; Nachum, O.; Yang, M. S.; Lee, L.; Freeman, D.; Guadarrama, S.; Fischer, I.; Xu, W.; Jang, E.; Michalewski, H.; et al. 2022. Multi-game decision transformers. *Advances in Neural Information Processing Systems*, 35: 27921–27936.

Levine, S.; Kumar, A.; Tucker, G.; and Fu, J. 2020. Offline reinforcement learning: Tutorial, review, and perspectives on open problems. *arXiv preprint arXiv:2005.01643*.

Liu, H.; and Abbeel, P. 2023. Emergent agentic transformer from chain of hindsight experience. In *International Conference on Machine Learning*, 21362–21374. PMLR.

Ma, Y.; HAO, J.; Liang, H.; and Xiao, C. 2024. Rethinking Decision Transformer via Hierarchical Reinforcement Learning. In *Forty-first International Conference on Machine Learning*.

Nair, A.; Gupta, A.; Dalal, M.; and Levine, S. 2020. Awac: Accelerating online reinforcement learning with offline datasets. *arXiv preprint arXiv:2006.09359*.

Newey, W. K.; and Powell, J. L. 1987. Asymmetric least squares estimation and testing. *Econometrica: Journal of the Econometric Society*, 819–847.

Rajeswaran, A.; Kumar, V.; Gupta, A.; Vezzani, G.; Schulman, J.; Todorov, E.; and Levine, S. 2017. Learning complex dexterous manipulation with deep reinforcement learning and demonstrations. *arXiv preprint arXiv:1709.10087*.

Rivenbark, A. G.; O’Connor, S. M.; and Coleman, W. B. 2013. Molecular and cellular heterogeneity in breast cancer: challenges for personalized medicine. *The American journal of pathology*, 183(4): 1113–1124.

Singla, A.; Rafferty, A. N.; Radanovic, G.; and Heffernan, N. T. 2021. Reinforcement learning for education: Opportunities and challenges. *arXiv preprint arXiv:2107.08828*.

Sutton, R. S.; and Barto, A. G. 2018. *Reinforcement learning: An introduction*. MIT press.

Tanaka, T.; Abe, K.; Ariu, K.; Morimura, T.; and Simo-Serra, E. 2024. Return-Aligned Decision Transformer. *arXiv preprint arXiv:2402.03923*.

Tarasov, D.; Nikulin, A.; Akimov, D.; Kurenkov, V.; and Kolesnikov, S. 2024. CORL: Research-oriented deep offline reinforcement learning library. *Advances in Neural Information Processing Systems*, 36.

Torabi, F.; Warnell, G.; and Stone, P. 2018. Behavioral cloning from observation. *arXiv preprint arXiv:1805.01954*.

Vaswani, A. 2017. Attention is all you need. *Advances in Neural Information Processing Systems*.

Wang, Y.; Yang, C.; Wen, Y.; Liu, Y.; and Qiao, Y. 2024. Critic-guided decision transformer for offline reinforcement learning. In *Proceedings of the AAAI Conference on Artificial Intelligence*, volume 38, 15706–15714.

Wang, Z.; Hunt, J. J.; and Zhou, M. 2022. Diffusion policies as an expressive policy class for offline reinforcement learning. *arXiv preprint arXiv:2208.06193*.

Wu, J.; Wu, H.; Qiu, Z.; Wang, J.; and Long, M. 2022. Supported policy optimization for offline reinforcement learning. *Advances in Neural Information Processing Systems*, 35: 31278–31291.

Wu, P.; Majumdar, A.; Stone, K.; Lin, Y.; Mordatch, I.; Abbeel, P.; and Rajeswaran, A. 2023. Masked trajectory models for prediction, representation, and control. In *International Conference on Machine Learning*, 37607–37623. PMLR.

Wu, Y.; Tucker, G.; and Nachum, O. 2019. Behavior regularized offline reinforcement learning. *arXiv preprint arXiv:1911.11361*.

Wu, Y.-H.; Wang, X.; and Hamaya, M. 2023. Elastic decision transformer. In *Proceedings of the 37th International Conference on Neural Information Processing Systems*, 18532–18550.

Xiao, C.; Wang, H.; Pan, Y.; White, A.; and White, M. 2023. The In-Sample Softmax for Offline Reinforcement Learning. In *The Eleventh International Conference on Learning Representations*.

Yamagata, T.; Khalil, A.; and Santos-Rodriguez, R. 2023. Q-learning decision transformer: Leveraging dynamic programming for conditional sequence modelling in offline rl. In *International Conference on Machine Learning*, 38989–39007. PMLR.

Zhang, H.; Xiao, C.; Wang, H.; Jin, J.; bo xu; and Müller, M. 2023. Replay Memory as An Empirical MDP: Combining Conservative Estimation with Experience Replay. In *The Eleventh International Conference on Learning Representations*.

Zhang, H.; and Yu, T. 2020. Taxonomy of reinforcement learning algorithms. *Deep reinforcement learning: Fundamentals, research and applications*, 125–133.

Zheng, Q.; Zhang, A.; and Grover, A. 2022. Online decision transformer. In *international conference on machine learning*, 27042–27059. PMLR.

Zhou, W.; Bajracharya, S.; and Held, D. 2021. Plas: Latent action space for offline reinforcement learning. In *Conference on Robot Learning*, 1719–1735. PMLR.

Appendix

A Outline

In this appendix, we provide the following supporting material in order: Appendix **B** details the full algorithm of *Doctor*; Appendix **C** provides additional justification of double-check mechanism and further discussion about our architecture design choice; Appendix **D** describes the environment details; Appendix **E** presents extended experimental results such as visualization examples, additional return-alignment plots, additional results, absolute error estimation; and Appendix **F** elaborates the model and training details; Finally, we discuss the limitations and the broader impact in Appendix **G** and Appendix **H**.

B Algorithm

The algorithm of *Doctor* can be found in Alg. 1. *Doctor* repeatedly samples trajectories and updates both a self-supervised reconstruction loss and a value loss during training. In the inference phase, at each timestep, it first samples N candidate returns, rolls out trajectories with the transformer, then double-checks each proposed next action by comparing its Q-value to the corresponding target return and picks the action whose value lies closest to the desired return. If online fine-tuning is enabled, actions may further be sampled from a Boltzmann distribution over Q-values to encourage exploration.

Algorithm 1: Double Checks the Transformer with Target Alignment for Offline RL (**Doctor**)

```

Input: Sequence buffer  $\mathcal{D}$ , Transformer models with weights  $\theta$ , networks  $Q$  with weights  $\phi$ 
// Training Phase
for number of training steps  $c = 0$  to  $C$  do
    Sample a batch of length  $K$  trajectories  $(\dots, R_t, s_t, a_t, r_t)$  from sequence buffer  $\mathcal{D}$ 
    Update the sum of supervised learning loss and value loss  $\mathcal{L}(\theta, \phi)$  via  $\mathcal{L}(\theta, \phi) = \mathcal{L}_{\text{recon}}(\theta) + \mathcal{L}_Q(\phi)$ .
end for
// Inference Phase
for environment steps  $t = 0$  to  $T$  do
    Initialize the environment  $s_0 \leftarrow \text{Env}$ 
    Randomly sample  $N$  returns via  $\{R_{t,1}, R_{t,2}, \dots, R_{t,N}\} \sim \text{Unif}(\delta(R_t), N)$ , and construct  $N$  trajectories
    Select the action with the nearest action-value to  $R_t$  according to  $a_{t,i} = \arg \min_{a_{t,i}} (|q_{t,i} - R_t|)$ .
    if online fine-tuning then
        Select action from Boltzmann distribution via  $\pi(a_t | s_t) = \frac{\exp(\beta q_{t,i})}{\sum_i \exp(\beta q_{t,i})}$ .
    end if
    Execute the action  $a_t$  in the environment and observe the reward  $r_t$  and next state  $s_{t+1}$ 
end for

```

C Discussion

C.1 Additional Justification of Double Check Mechanism

Assume our action-value function is optimal, $Q = Q^*$. We select the action a_t that minimizes the absolute difference between the predicted action-value and the desired return:

$$a_t = \arg \min_a |Q^*(s_t, a) - R_t|. \quad (11)$$

We show that this action selection aligns the expected return with R_t , achieving return alignment.

Case 1: $R_t > R$ (desired return exceeds achievable return)

The desired return R_t is greater than the maximum possible return $R = V^*(s_t)$, where:

$$V^*(s_t) = \max_a Q^*(s_t, a) \quad (12)$$

Since $Q^*(s_t, a) \leq V^*(s_t)$ for all actions a , we have:

$$Q^*(s_t, a) - R_t \leq V^*(s_t) - R_t < 0 \quad (13)$$

The absolute difference $|Q^*(s_t, a) - R_t|$ is minimized when $Q^*(s_t, a)$ is maximized. The optimal action a^* is $a^* = \arg \max_a Q^*(s_t, a)$. Selecting $a_t = a^*$ minimizes $|Q^*(s_t, a) - R_t|$. Even when R_t is not attainable, the method selects the action that yields the highest possible return.

Case 2: $R_t < R$ (desired return less than achievable return)

The desired return R_t is less than the maximum possible return $R = V^*(s_t)$. There may exist actions a such that $Q^*(s_t, a) \approx R_t$. By minimizing $|Q^*(s_t, a) - R_t|$, we may select an action a_t where $Q^*(s_t, a_t) \geq R_t$ but potentially less than $V^*(s_t)$. This action aligns the expected return with R_t without necessarily maximizing it and allows for controlled performance.

C.2 Additional Explanation for the Design Choice

Transformer Architecture. Early works like DT (Chen et al. 2021) and TT (Janner, Li, and Levine 2021) rely on causal transformers, which predict each subsequent token based on past tokens. Recent studies such as MTM (Wu et al. 2023) demonstrated that bidirectional transformers trained with a mixture of random and auto-regressive masking achieve good performance. Random masks encourage the model to reconstruct missing tokens by leveraging the context of the unmasked sequence, enhancing the reconstruction and generalization abilities. Our experiments also demonstrate that the bidirectional-based MTM outperforms DT, exhibiting stronger interpolation when handling trajectories associated with underrepresented returns. Our proposed model further enhances these benefits, resulting in improved return alignment.

Q-function Learning. To learn the Q-function, we employ expectile regression (Kostrikov, Nair, and Levine 2022). When the expectile parameter $\nu > 0.5$, the resulting loss function assigns lower weight to errors arising from underestimated Q-values. This asymmetric allows us to approximate $Q(s, a) \leftarrow r + \gamma \max_{(s', a') \in \mathcal{D}} Q(s', a')$, achieving reliable in-sample learning. This precision is especially critical for our double-check mechanism, which is dependent on accurate Q-value predictions within data-supported regions, selecting actions closely aligned with the target return.

C.3 Difference Between *Doctor* and Previous Methods

RvS fails to achieve one of the desired properties of offline RL agents, stitching. To enhance transformers with stitching ability, QDT (Yamagata, Khalil, and Santos-Rodriguez 2023) relabels the Return-to-Go in the dataset by learning a conservative value function, serves as data augmentation by incorporating stitched trajectories into the training dataset. EDT (Wu, Wang, and Hamaya 2023) optimizes the trajectory by retaining a longer history when the previous trajectory is optimal and a shorter one when it is sub-optimal, enabling it to stitch with a more optimal trajectory. ACT (Gao et al. 2024) and CGDT (Wang et al. 2024) uses learned Q-values to guide actions or as critic prompts. QT (Hu et al. 2024) and QCS (Kim et al. 2024) impose a regularizer of the Q-value during transformer training.

Different from these previous methods, which mainly focus on improving the model’s stitching ability to obtain the best policy from the dataset. Our primary objective is explicit target alignment, enabling a single offline trained transformer to perform accurately at different policy expertise. Technically, unlike previous methods that learn the value functions beforehand and train the SL model separately afterward, *Doctor* let the value function utilize the representation feature of the transformer base model. And we perform test-time scaling of the outputs, combined with value function verification to ensure alignment.

D Environment Details

D.1 D4RL

Gym Locomotion. The D4RL Gym locomotion benchmark (Fu et al. 2020) includes environments provided by OpenAI Gym (Brockman 2016), specifically Walker2d, Hopper, and HalfCheetah. Each task is configured with three levels of dataset difficulty: Medium-Replay, Medium, and Medium-Expert. The Medium dataset corresponds to policies performing at approximately one-third of expert-level performance, while the Medium-Replay dataset contains the replay buffer from an agent trained to medium-level performance. The Medium-Expert dataset combines trajectories generated by both medium and expert policies. These environments are widely used for evaluating reinforcement learning algorithms. For example, Walker2d environment simulates a robot tasked with walking as fast and as stably as possible. The robot must coordinate its two legs to achieve efficient locomotion without falling over. These environments are designed to test an agent’s ability to learn complex motor skills and optimize control strategies.

Adroit (Rajeswaran et al. 2017). Adroit is a suite of dexterous manipulation tasks designed to simulate the control of a five-fingered robotic hand. Our experiments focus on three tasks from this suite: Pen, Door, and Hammer. For example, the Pen task involves rotating a pen to a specific orientation using the robotic hand’s dexterous manipulation skills. The cloned tasks used in our experiment collect a 50-50 split of demonstration data and 2500 trajectories sampled from a behavior cloning policy.

Maze2D. Maze2D is a navigation task in which the agent is required to reach a fixed target position. These tasks are designed to evaluate the ability of offline reinforcement learning algorithms to stitch together different trajectory fragments (Fu et al. 2020). We used three environments included in Maze2D, umaze, medium, and large, with complexity and path length to the target increasing sequentially.

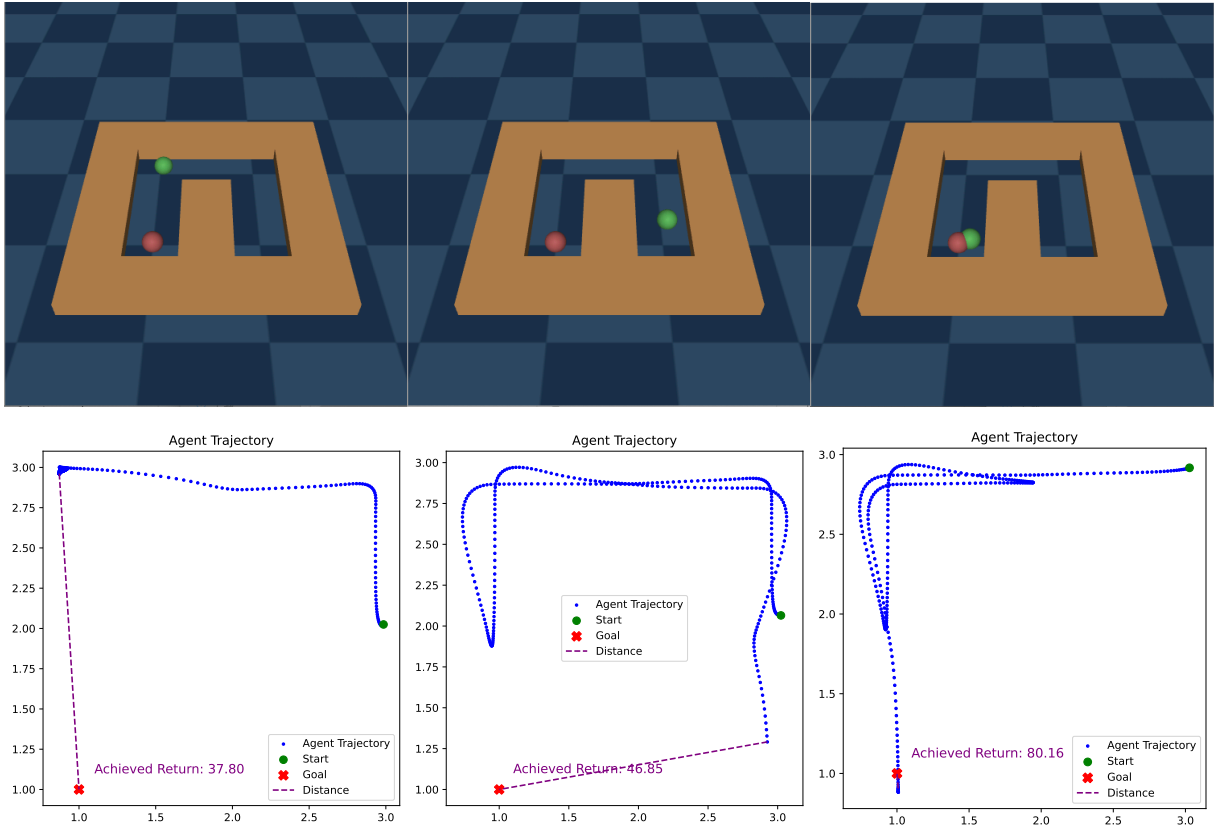


Figure 7: Trajectories generated under three different target returns, which are 10, 40 and 80, respectively, from the left to right. The first row shows the frames near the end of the trajectories, while the second row displays the corresponding trajectories produced by the inference model. As the target return increases, we observe that the agent is guided closer to the goal

D.2 EpiCare

Environment. EpiCare (Hargrave, Spaeth, and Grosenick 2024) is a flexible yet clinically motivated benchmark to evaluate offline RL and safety-aware decision making in dynamic treatment regimes. EpiCare frames longitudinal patient care as a finite-horizon POMDP (Kaelbling, Littman, and Cassandra 1998). The hidden state space $S = \{s_r, s_a, s_1, \dots, s_{n_s}\}$ contains n_s disease states plus terminal remission (s_r) and adverse event (s_a) states, the discrete action set $A = \{a_1, \dots, a_{n_a}\}$ represents treatments, and the observation space $O = [0, 1]^{d_o}$ records d_o separate symptoms that the clinician sees. Disease progression obeys a transition function T that is multiplicatively modulated by each treatment's vector m_a , together with treatment-specific remission probabilities $T(s_r | s_i, a)$ and an observation-triggered adverse-event rule, this yields the transition function:

$$T(s_j | s_i, a) = (1 - T(s_r | s_i, a) - T(s_a | s_i, a)) \frac{(m_a)_j T_{i,j}}{\sum_k (m_a)_k T_{i,k}}. \quad (14)$$

Observations are generated by adding a treatment-specific symptom shift δ_a to a state-dependent Gaussian draw \tilde{o} , then applying: $o = [\expit(\tilde{o} + \delta_a)]_1$. capturing measurement noise and treatment side effects. The reward function is

$$R(s, a, o) = \begin{cases} r_r, & s = s_r \\ r_a, & s = s_a \\ -c_a - c_o \sum_i o_i, & \text{otherwise} \end{cases} \quad (15)$$

where $r_r > 0$ rewards remission, $r_a = -r_r$ penalizes adverse events, c_a encodes treatment cost and c_o prices symptom cost. An episode starts from an initial distribution derived from the stationary mix of the Markov graph and ends in remission, an adverse event, or after a maximum of treatment steps. Each random environment seed automatically instantiates new state graphs, symptom distributions, and treatment parameters.

Behavior Policy. The Standard-of-Care (SoC) policy seeks immediate benefit while avoiding harm, which is used to collect data on the EpiCare benchmark in our experiment. The SoC policy emulates a risk-averse clinician who ignores the hidden

disease state and instead tracks the instantaneous value of each treatment as a multi-armed bandit. It resets the estimate to the expected reward $Q_0(a) = \mathbb{E}[R | a]$, then updates it after each dose with an exponentially recency-weighted rule

$$Q_{t+1}(a) = \begin{cases} Q_t(a) + \alpha (R_t - Q_t(a)), & a = a_t \\ Q_t(a), & a \neq a_t \end{cases}, \quad (16)$$

To protect the patient, SoC greedily selects the reward-maximising action within the safe set $A_{\text{safe}}(o) = \{a \in A : (\delta_a)_i \leq 0 \text{ for all } i \text{ with } o_i \geq 1 - \frac{\kappa}{2}\}$, thereby refusing any drug that would further elevate a symptom already above the danger threshold κ .

E Additional Experimental Results

E.1 Visualization Example for Return Alignment

In this section, we provide an intuitive toy demonstration to illustrate the efficacy of return alignment achieved by *Doctor*. We record the gif on the maze2d-umaze-dense task. The Maze2D dataset contains suboptimal trajectories and is specifically designed to evaluate the stitching ability. Supervised learning-based methods, such as DT, struggle when faced with suboptimal trajectories. As a reference, the normalized return of DT in this environment is -6.8, indicating a complete collapse in performance (Yamagata, Khalil, and Santos-Rodriguez 2023).

We save the model parameter of *Doctor* trained offline and evaluate in this environment, where each rollout is limited to 300 steps. We present trajectories generated under three different target returns. The first row of Figure 7 shows the frames near the end of the trajectories, while the second row displays the corresponding trajectories produced by the inference model. As the target return increases, we observe that the agent is guided closer to the goal. For example, when the target return is 80, the agent is closer to the goal than when the target return is 40. In this environment, since the reward is the exponential negative Euclidean distance between the achieved goal position and the desired goal, even if the agent remains stationary, it will still receive a positive return. Interestingly, when the target return is 40, the ball exhibits higher acceleration compared with the target return of 10, traveling further, while the actual return is controlled to achieve the target return precisely. When the target return is 80, the ball ultimately chooses to achieve a higher return and reaches the place near the goal.

E.2 Additional Results for Return Alignment

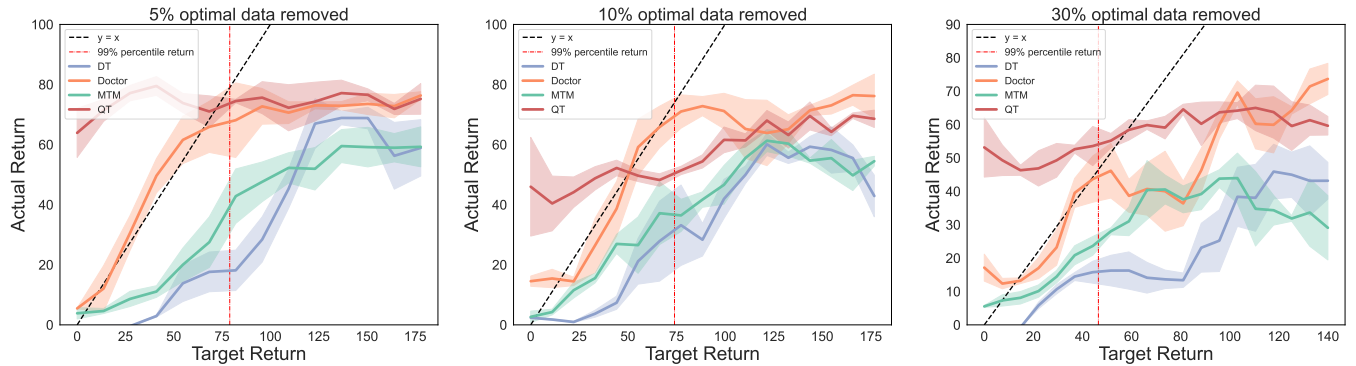


Figure 8: We evaluate the alignment ability of *Doctor* on the walker2d-medium-replay-v2 with the top returns of trajectories removed. *Doctor* achieves much better alignment across a wide range of target returns compared to DT, MTM and QT.

In our additional results as shown in Figure 8, we evaluated the return alignment capabilities of *Doctor* under conditions where optimal data was removed. Notably, even with the removal of the top 5% of the highest-quality data, traditional RvS methods such as MTM and DT exhibited significant performance degradation, both in terms of extrapolation and interpolation. QT, by incorporating a Q-value regularizer, enhanced its stitching ability and demonstrated robust performance in maximizing the expected return. However, this improvement appeared to come at the cost of reduced interpolation accuracy and struggled to precisely align with the target return. Remarkably, *Doctor* consistently achieved the best alignment performance, closely adhering to the ideal line and outperforming all other methods in maintaining precise alignment.

E.3 Complex Control Tasks

In addition to evaluation in the MuJoCo domain, we further assess *Doctor* in the challenging Adroit tasks, which consist of three dexterous control tasks, each requiring precise interactions and hand-object coordination. As shown in Table 4, we compare both RvS methods (DT, MTM) and value-based algorithms (CQL, IQL, TD3+BC) as well as the recent combination method

Adroit Tasks	BC	CQL	IQL	TD3+BC	DT	MTM	QT	Doctor
pen-cloned	37.0	39.2	37.3	5.1	75.8	80.5	91.5	98.4\pm15.5
hammer-cloned	0.6	2.1	2.1	-0.3	3.0	5.3	12.2	5.9 \pm 3.1
door-cloned	0.0	0.4	1.6	0.2	16.3	17.4	21.1	24.2\pm8.7
Adroit Sum	37.6	41.7	41.0	5.0	95.1	103.2	124.8	128.5

Table 4: Offline results in the Adroit domain. *Doctor* achieves competitive or superior results compared to the baselines.

QT. In the Pen and Door environment, *Doctor* outperforms other baselines, demonstrating *Doctor*'s robustness in a range of tasks with varying features.

E.4 Stitching Ability

Maze2D Tasks	BC	CQL	IQL	TD3+BC	DT	MTM	QDT	Doctor
maze2d-umaze	88.9	94.7	42.1	14.8	31.0	40.2	58.6	97.2\pm9.8
maze2d-medium	38.3	41.8	34.9	62.1	8.2	26.5	42.3	106.2\pm7.3
maze2d-large	1.5	49.6	61.7	88.6	2.3	9.8	62.2	75.7\pm6.4
Maze2d Sum	128.7	186.1	138.7	165.5	41.5	76.5	163.1	279.1

Table 5: Offline results in the maze2d domain. *Doctor* achieves competitive or superior results compared to the baselines.

We also evaluate *Doctor* in the Maze2D suite, a classic benchmark for testing an offline agent's ability to stitch together short sub-trajectories into a coherent high-return path. Maze2D comprises three tasks of increasing difficulty (umaze, medium, large). As reported in Table 5, RvS-based approaches (DT, MTM) collapse or do not fully exploit the data. *Doctor* outperforms other baselines including value-based methods that are good at stitching, clearly demonstrating its stitching ability.

E.5 Additional Results on EpiCare

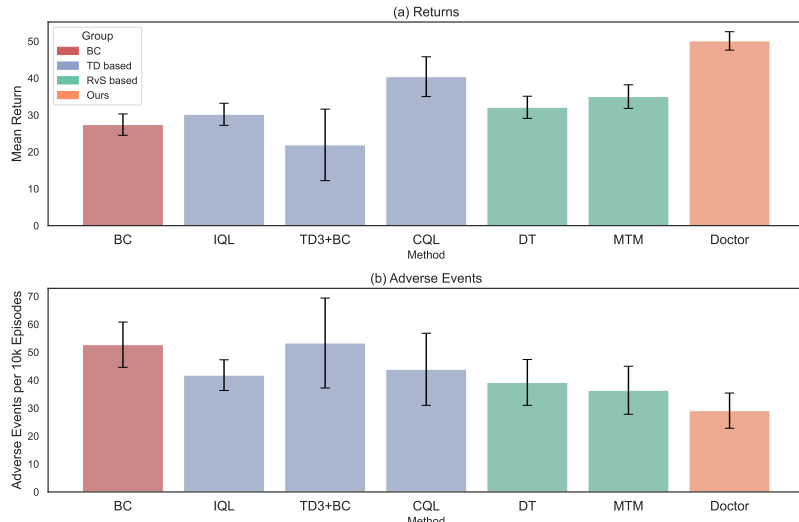


Figure 9: Mean returns of and number of adverse events per 10k episodes (lower is better) for each offline learning method on the SoC dataset, averaged over eight structurally distinct EpiCare environments (environment seeds 1–8). Error bars denote standard deviation.

Figure 9 reports the mean returns and the number of adverse events (lower is better) for each offline learning method on the SoC dataset, averaged over eight structurally distinct EpiCare environments (environment seeds 1–8). Error bars denote standard deviation. *Doctor* achieves the lowest adverse events and the best clinical returns, outperforming other baselines

and demonstrating that *Doctor*'s alignment produces substantially safer and more effective treatment policies on the dynamic treatment regime benchmark.

E.6 Error Between the Actual Return and the Target Return

Dataset	DT	RADT	QT	<i>Doctor</i>
halfcheetah-MR	7.2	1.8	20.2	5.0 ± 3.9
hopper-MR	12.2	4.4	15.4	8.1 ± 5.1
walker2d-MR	8.1	4.0	28.1	7.5 ± 6.6
halfcheetah-M	36.9	36.3	30.5	16.2 ± 4.9
hopper-M	16.3	6.5	17.6	10.4 ± 3.3
walker2d-M	23.6	10.8	36.8	12.0 ± 7.5
	104.3	63.8	148.6	59.2

Table 6: Absolute error comparison in the Locomotion tasks. We report the average absolute error over target returns. The results are averaged over three random seeds. Lower summation is better. *Doctor* achieves comparable performance with RADT in terms of minimizing absolute error.

In this section, we evaluate the absolute error between the actual return and the target return of *Doctor*. We compare *Doctor* with other RvS-based baselines. The absolute error is calculated using the following formula:

$$E_{\text{diff}}(R_{\text{target}}, R_{\text{actual}}) = \left| R_{\text{target}} - \sum_{t=1}^T r_t \right|. \quad (17)$$

We report the final absolute error over 3 random seeds in Gym locomotion-v2 tasks as shown in Table 6. The target return is set to 0x-1.0x times the maximum return in the dataset. We put the maximum return of the different dataset in Table 7. According to the table, DT and QT have large absolute error across varying targets. *Doctor* effectively aligns the actual return with the target return and achieves competitive performance with RADT in terms of minimizing absolute error.

Dataset	max R	mean R	normalized max R
hopper-M	3222	1422	99.5
hopper-MR	3192	467	98.6
halfcheetah-M	5309	4770	45.0
halfcheetah-MR	4985	3093	42.4
walker2d-M	4226	2852	92.0
walker2d-MR	4132	682	89.9

Table 7: Scores in Gym locomotion datasets. This table shows maximum return, mean return and normalized return for each dataset.

E.7 Additional Results for Online Finetuning

Locomotion Tasks	IQL	MTM-O	ODT	<i>Doctor</i>
HalfCheetah-MR	44.2 → 44.5	43.0 → 43.4	40.0 → 41.2	$46.6 \rightarrow 42.4 \pm 0.9$
Hopper-MR	94.7 → 97.5	92.9 → 94.6	86.6 → 91.3	98.8 → 98.6 ± 2.0
Walker2d-MR	73.9 → 79.2	77.3 → 82.1	68.9 → 78.4	86.2 → 88.5 ± 5.4
HalfCheetah-M	47.4 → 47.1	43.6 → 45.2	42.7 → 43.6	$48.4 \rightarrow 44.3 \pm 1.8$
Hopper-M	66.3 → 80.1	64.1 → 70.2	66.9 → 98.1	$85.6 \rightarrow 93.5 \pm 5.1$
Walker2d-M	78.3 → 81.9	70.4 → 71.0	72.2 → 77.0	81.1 → 84.7 ± 3.7
Sum	404.8 → 430.3	391.3 → 406.5	377.3 → 429.6	446.7 → 452.0

Table 8: Online fine-tuning results. We report the average returns after 1 million online interactions. *Doctor* observes clear improvements on Hopper-M.

Transformer Policy	Value
Encoder layers	2
Decoder layers	1
Activation function	GeLu
Number of attention heads	4
Embedding dimension	512
layers of decoding head	2
Dropout	0.10
Positional encoding	Yes
Dropout	0.1
Learning rate	0.0001
Weight decay	0.005
Betas	[0.9,0.999]
Learning rate warmup steps	20000
<i>Q</i> Value Heads	Value
Number of layers	2
Activation function	ReLU
Embedding dimension	256
Tau	0.7 for Locomotion, 0.9 for Maze2d and 0.8 for Adroit and EpiCare
Learning rate	0.0001
Weight decay	5e-4
General	Value
Eval episodes	10
Input trajectory length	4
Trainning steps	140000
Batch size	512
Discount factor	0.99

Table 9: Hyperparameters of *Doctor* in experiments

In this section, we further investigate whether the double-check mechanism can help the base transformer model to explore novel states in the environment for fine-tuning, thereby boosting performance. During online exploration, actions are sampled based on a desired target return, indicating the area we wish to explore. The Q function then evaluate these actions, providing prior knowledge about potential actions. For example, we can select actions from the Boltzmann distribution based on the Q function,

$$\pi(a_t|s_t) = \frac{\exp(\beta q_{t,i})}{\sum_i \exp(\beta q_{t,i})}, \quad (18)$$

where β is a temperature parameter that controls the sharpness of the distribution. This results in an effective exploration strategy that integrates prior knowledge from the value functions and the desired target returns, as summarized in Alg. 1.

We evaluate this in an online setting, aimed to test whether the model can further improve by interacting with the environment. We maintain the top 5% of the trajectories in the dataset and further interact with the environment for 1 million steps, which corresponds to approximately 1500 episodes. We sample actions based on Eq. 18 and set target returns dynamically as the maximum return R_{\max} in the dataset and $\delta = 2R_{\max}$, $\beta = 100$. Each time after rolling out for one episode, we perform 200 gradient updates based on the collected data.

As shown in Table 8, *Doctor* achieves a performance improvement on some tasks when incorporating additional online interaction data. ODT (Zheng, Zhang, and Grover 2022) is a DT-based variant trained with sequence-level entropy regularization for offline-to-online fine-tuning. MTM-O is an online variant of MTM we implement for test its ability of fintuning. *Doctor* outperforms ODT and IQL in several tasks, with clear improvements in performance on Hopper-M. This demonstrates the effectiveness of the double-check mechanism for online fine-tuning, allowing the model to explore effectively. The availability of online data can further improve the performance of transformer models.

F Model and Training Details

F.1 Model Hyperparameters and Baseline Details

We build our policy and Q value heads as a transformer-based model. The detailed model hyperparameters are in Table 9.

For DT, we train the model using the setting inherit from CORL (Tarasov et al. 2024). We inherit the QT settings from the source code provided by the original paper authors. Model parameters of QT and DT are given in Table 10.

Parameter	Value
Number of layers	4
Number of attention heads	4
Embedding dimension	512
Nonlinearity function	ReLU
Batch size	256
Context length K	20
Dropout	0.1
Learning rate	3e-4

Table 10: Hyperparameters of QT/DT in experiments.

F.2 Training Details

We provide implementation details of *Doctor*. The supervised learning model include a bidirectional transformer encoder and a bidirectional transformer decoder. Before inputting the sequence data into the model, each input modality is projected into the embedding space through independent embed-encodings. The output of the decoder is connected to a 2-layer MLP with layer normalization, which is used to reconstruct the trajectory sequence. The Transformer is trained with a randomly sampled series of mask ratios similar to (Wu et al. 2023): $\text{mask_ratios} = [0.6, 0.7, 0.8, 0.85, 0.9, 0.95, 1.0]$. For data sampling, we adopt a two-step sampling method similar to that used in DT (Chen et al. 2021), where we first sample a single trajectory and then uniformly sample sub-trajectories of a certain sequence length.

For offline training, we initialize the AdamW optimizer for the Transformer model and the Adam optimizer for the Q -value head, employing both warmup and decay schedules. The Q -value head consists of two 256-dimensional MLP layers, which connect to the output of the transformer decoder. All hyperparameters are summarized in Table 9.

During the fine-tuning stage, we initialize the replay buffer with the top 5% highest-return trajectories from the offline dataset. Each time we interact with the environment, we fully roll out one episode using the current policy and add it to the replay buffer. We then update the policy and roll out again, following a process similar to (Zheng, Zhang, and Grover 2022).

G Limitations

In this paper, we introduce *Doctor* to address the return-alignment problem and demonstrate its effectiveness on standard RL benchmarks such as MuJoCo, Maze2d, Adroit, and EpiCare. Although EpiCare captures many real-world clinical challenges, such as short treatment horizons, heterogeneous treatment effects, partial observability, and adverse events, it remains a simulated environment. As a next step, we plan to evaluate our method on real-world clinical datasets.

H Broader Impacts

This study focuses on improving the alignment accuracy of RvS methods in offline reinforcement learning. By addressing their current limitations and achieving a closer match between actual and target returns, it advances the field of offline reinforcement learning. As foundational machine learning research, it poses no negative societal impacts.